PNAS RESEARCH ARTICLE | ECOLOGY

Kelp forest collapse alters the reef microbiome and associated metabolome

Shane P. Farrell[a,b,1], Timothy D'Angelo[a], Dara S. Yiu[a,b], Abzer Kelminal Pakkir Shah[c,d], Paolo Stincone[d], Peter D. Countway[a], Daniel Petras[c,d], Damian C. Brady[b], and Douglas B. Rasher[a,1]

Affiliations are included on p. 9.

Edited by Alan Hastings, University of California Davis, Davis, CA; received October 13, 2025; accepted July 19, 2026

In many temperate regions experiencing rapid ocean warming, kelp forests are being replaced by low-lying turf algae. Yet, whether this change in biogenic habitat alters reef-level microbial structure and function, including carbon and nutrient cycling, remains largely unknown. Here, we integrated shotgun metagenomics and nontargeted metabolomics to reveal that kelp forest loss alters the composition of the reef microbial community and its associated biochemical machinery, resulting in distinct metabolomes and microbially driven elemental use/transformations on kelp- vs. turf-dominated reefs. Our results therefore suggest that microbes play a key role in shaping kelp forest ecosystem functioning. Further, they demonstrate that human-induced ocean warming has cascading effects on microbially mediated chemistry, with implications for coastal carbon storage and nutrient regeneration.

state shift | kelp | turf | microbiome | climate change

Significance

Temperate coastal ecosystems are undergoing rapid change where ocean warming has triggered the collapse of kelp forests and proliferation of low-lying turf algae. Here, we investigated how this ecosystem state shift alters the composition of the reef microbial community and its biochemical machinery, along with the reef's chemical landscape (i.e., metabolome). We identified that the kelp-to-turf transition is associated with a change in the taxonomy and function of the reef microbial community, which in turn alters microbe–chemical interactions on the reef and the resultant metabolome. This study provides insights into how human-induced ocean warming changes the microbiome–the "unseen majority"–of temperate reefs, and reveals the implications of this change for carbon and nutrient dynamics.

Ecosystem state shifts, whereby habitat-forming foundation species are lost, are known to disrupt biodiversity, ecosystem function, and key services that support human well-being (1). Climate change and other human-induced stressors have amplified the frequency and severity of these state shifts in both terrestrial (e.g., savanna-to-grassland, woodland-to-boreal) and marine (e.g., coral-to-macroalgae, saltmarsh-to-mudflat, kelp forest-to-urchin barren) ecosystems (2–4). Yet, despite the global prevalence of ecosystem state shifts, our knowledge of how microbial communities respond to such events is limited to very few biomes (5, 6).

For example, although cold-water kelp forests are collapsing and being replaced by low-lying mats of turf algae in many areas of rapid ocean warming (7), the consequences of this state shift for reef microbial dynamics remain unclear. The kelp-to-turf state shift, documented in Australia (8), Japan (9), the Mediterranean Sea (10), the Baltic Sea (11), and the Northeast and Northwest Atlantic Oceans (12–16), is associated with biodiversity loss, altered nutrient cycling, and diminished recovery potential for kelp populations (8, 9, 16–21). However, unlike tropical coral reef and seagrass ecosystems, where microbial dynamics are well documented, we know little about how microbial communities change during kelp-to-turf transitions, or whether such changes alter key ecosystem-level processes.

Furthermore, we have little understanding of how changes in microbial communities interact with dissolved organic matter (DOM) pools on temperate reefs. Produced by benthic macroalgae (kelp, turf) and microbial metabolism, DOM forms an essential part of the ocean's carbon pool and regulates nutrient cycling, energy flow, and microbial community composition (22). As reef dwelling species change in relative dominance, so does the composition of the DOM pool (23). For example, DOM composition is altered when tropical coral reefs shift to macroalgal dominance, whereby macroalgae produce more energy-rich exudates, which in turn stimulate fast-growing bacteria that alter reef-level metabolism (5, 24). Likewise, in terrestrial ecosystems, shifts in organic matter composition due to vegetation changes select for microbial taxa that accelerate carbon loss and alter nutrient cycling (25). These examples underscore how shifts in DOM can mediate microbial responses and ecosystem-level changes following habitat loss.

Here, we explored how kelp forest collapse is altering reef microbial diversity, community composition, and functional potential in the Gulf of Maine, where a kelp-to-turf transition is unfolding due to rapid ocean warming. In recent decades, the southwestern Gulf experienced rapid kelp forest loss and a shift to turf algae, whereas kelp forests continue to persist in the northeastern Gulf (14, 16). Moreover, in this region, turf-dominated reefs harbor unique DOM pools relative to kelp forests (21). As such, this region provides an ideal setting to investigate how changes in biogenic habitat—from massive kelps to diminutive turf algae—influence microbial communities, DOM pools, and their interaction.

Author contributions: S.P.F. and D.B.R. conceived and designed the research; S.P.F., D.S.Y., P.S., and D.B.R. performed the research; S.P.F., A.K.P.S., P.S., P.D.C., D.P., D.C.B., and D.B.R. contributed new reagents/analytic tools; S.P.F., T.D., A.K.P.S., P.S., and D.P. analyzed the data; and S.P.F., T.D., and D.B.R. wrote the paper.

The authors declare no competing interest.

This article is a PNAS Direct Submission.

Copyright © 2026 the Author(s). Published by PNAS. This article is distributed under Creative Commons Attribution-NonCommercial-NoDerivatives License 4.0 (CC BY-NC-ND).

PNAS policy is to publish maps as provided by the authors.

[1]To whom correspondence may be addressed. Email: Shanepfarrell@gmail.com or drasher@bigelow.org.

This article contains supporting information online at https://www.pnas.org/lookup/suppl/doi:10.1073/pnas.2525548123/-/DCSupplemental.

Published August 31, 2026.

Downloaded from https://www.pnas.org by Douglas Rasher on September 2, 2026 from IP address 172.83.249.35.

Specifically, using shotgun metagenomics, we compared microbial i) taxonomic and ii) functional diversity, structure, and differential abundance between reef ecosystem states, as well as iii) determined which microbial taxa drove the functional differences we identified. Then, using nontargeted metabolomics, we iv) assessed correlations between microbial communities and DOM pools, and v) documented differences in ecologically relevant chemistry on kelp- vs. turf-dominated reefs. Our data indicate that kelp forest loss reshapes microbial community structure and DOM processing, with implications for ecosystem-level carbon and nutrient cycling.

Results

The Effects of Kelp Forest Collapse on Microbial Diversity and Community Structure. Previous studies have described microbial communities associated with the surfaces of kelp, yet we aimed to characterize them on the reef–where key species interactions occur. Thus, we sampled reef biofilms, and did so on three replicate kelp-dominated reefs and three replicate turf-dominated reefs in May/June (hereafter "spring") and August/September (hereafter "summer") of 2022 (Fig. 1*A*). We then performed shotgun metagenomic sequencing. During both sampling periods, microbial communities on both kelp-dominated reefs and turf-dominated reefs were defined by four phyla (Bacteroidota, Planctomycetota, Pseudomonadota, and Verrucomicrobiota), which collectively accounted for ~80% of abundance across all samples (*SI Appendix*, Fig. S1). Core families shared between kelp- and turf-dominated reefs–defined as those with a relative abundance > 5% and present in > 70% of samples within each reef state–were Akkermansiaceae, Flavobacteriaceae, and Rhodobacteraceae (*SI Appendix*, Fig. S2).

In summer (when water temperatures are at their maximum and reef communities are fully developed in the Gulf of Maine; Fig. 1*B*), microbial community compositions were distinct on kelp- vs. turf-dominated reefs (PERMANOVA based on Euclidean distance, $P < 0.05$; Fig. 1 *C* and *D* and *SI Appendix*, Tables S1 and S2). Taxa

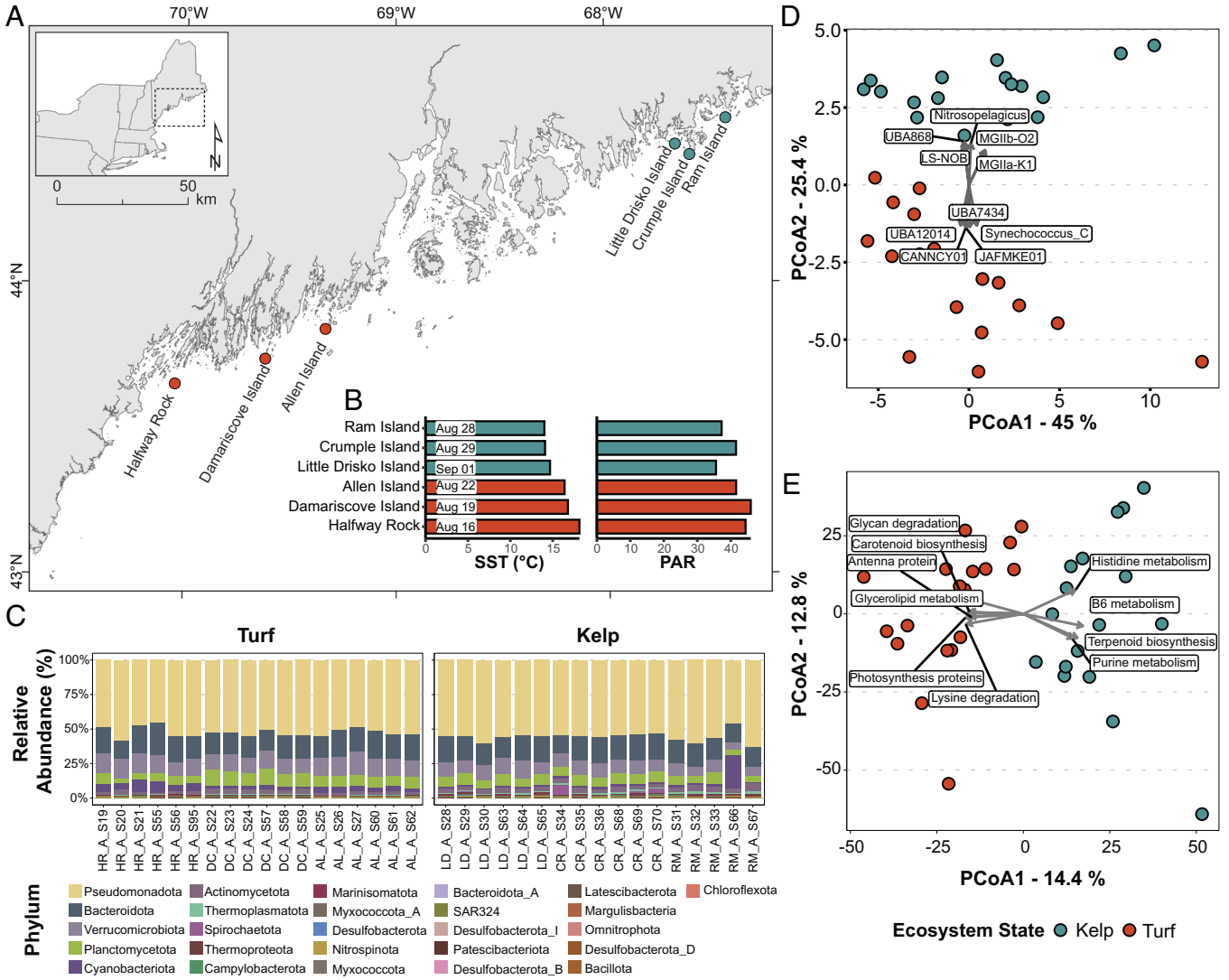


Fig. 1. Distinct microbial taxonomy and function between kelp forests and turf-dominated reefs. (*A*) Map of study sites across Maine's coast which include replicate sites in southwestern Maine where kelp forests have collapsed and been replaced by filamentous turf algae and sites in northeastern Maine where kelp forests persist. Adapted from ref. 21. (*B*) Sea surface temperature (°C) and photosynthetically active radiation (μmol photons m^{-2} s^{-1}) at the study sites during summer collections. (*C*) Relative abundance of microbial phyla within turf reefs and kelp forests during summer sampling. (*D*) Ordination of microbial taxonomic beta diversity associated with kelp-dominated (blue) vs. turf-dominated (red) reefs in summer (Euclidean distance; PERMANOVA, $P < 0.05$; Dispersion $P > 0.05$). (*E*) Ordination of microbial functional beta diversity associated with kelp- and turf-dominated reefs in summer (Euclidean distance; PERMANOVA, $P < 0.05$; Dispersion $P > 0.05$). Vectors depict the dominant taxa (*D*) or microbial metabolic functions (*E*) driving separation. In panel *C*, samples are ordered by site, from southwest to northeast (HR: Halfway Rock, DC: Damariscove Island, AL: Allen Island, LD: Little Drisko Island, CR: Crumple Island, RM: Ram Island) and include a unique identifier.

Downloaded from https://www.pnas.org by Douglas Rasher on September 2, 2026 from IP address 172.83.249.35.

driving these distinctions included nitrogen fixing and transforming taxa (*MGIIb-O2*, *MGIIb-K1*, and *Nitrosopelagicus*) within kelp forests, and photosynthetic and heterotrophic taxa (*Synechococcus* and Pseudomonadales) on turf-dominated reefs (Fig. 1*D*). Such distinctions between kelp- and turf-dominated reefs were also evident in spring–when seawater temperatures were virtually the same across all study sites (*SI Appendix*, Figs. S3–S6)–suggesting that differences in summer microbial composition were, in large part, driven by disparities in biogenic reef habitat.

The Effects of Kelp Forest Collapse on Microbial Functional Potential. Investigating our metagenomic data, we made use of KEGG Orthology (KO) annotations to map out the functional potential of each microbial species. We identified a core set of gene functions (> 1% relative abundance and present in > 70% of samples) common to microbes on both kelp- and turf-dominated reefs. Core functions were primarily associated with essential genetic processes, including noncoding RNAs, various transporters, and transcription factors (*SI Appendix*, Fig. S7). These core functions likely support cellular activities such as protein synthesis, signaling, and metabolite transport, which are crucial for microbe survival (26).

Yet, KO analysis also revealed distinct differences in the metabolic functional potential of microbes associated with kelp- vs. turf-dominated reefs (Fig. 1*E*). Kelp forests were differentiated by microbes with enriched purine metabolism, terpenoid backbone biosynthesis, and vitamin B6 metabolism, whereas turf reefs were differentiated by microbes with functional pathways related to photosynthesis, antenna proteins, and carotenoid biosynthesis (which may signal a shift to photosynthesis as a primary energy source) (Fig. 1*E*).

Differentially Abundant Taxa and Functions between Ecosystem States. On kelp-dominated reefs, the most differentially abundant genera were Archaea, namely *MGIIb-O2*, *Nitrosopelagicus*, *MGIIa-L1*, *Nitrosopumilus*, *MGIIa-L2*, and *MGIIa-K1* (Fig. 2 *A* and *B*). In contrast, turf-dominated reefs harbored a differential abundance of bacterial taxa, including *Polaribacter*, *Pelagibacter*, *Synechococcus,* and *Planktomarina* (Fig. 2 *A* and *B*). Thus, the transition from kelp- to turf-dominance results in an interdomain shift in relative abundance, with archaeal taxa declining and bacterial taxa (particularly photosynthetic *Synechococcus*) becoming more prevalent (Fig. 2*C* and *SI Appendix*, Fig. S8).

Furthermore, using compositionally aware differential abundance analysis, we found that 11.8% of all annotated gene functions (9,609 total) were differentially abundant between kelp- and turf-dominated reefs in summer. In kelp forests, microbial communities were enriched in metabolic functions related to amino acid, carbohydrate, energy, and nucleotide metabolism, whereas turf reef microbial communities were enriched in gene functions related to lipid metabolism, secondary metabolite production, and vitamin biosynthesis (Fig. 2*D*). Notably, a substantial number of gene functions related to energy metabolism were differentially abundant on turf-dominated reefs (Fig. 2*D*).

The most pronounced differences in those functions related to energy metabolism were associated with photosynthesis (Fig. 2*E*). Microbial communities on turf-dominated reefs were enriched in pathways related to photosynthesis, photosynthesis proteins, and antenna proteins (Fig. 2*E*), reflecting a shift to more phototrophic microbial communities that may capitalize on abundant light in turf habitats following a loss of the kelp forest canopy. On the other hand, microbial communities on kelp-dominated reefs were enriched in nitrogen metabolism and oxidative phosphorylation functions hosted by Archaea, such as ammonia monooxygenase subunit B (K10945) and the Archaeal V/A-type ATPases (K02123, K02119, and K02120) (Fig. 2*E*).

Microbes That Underpin Differentially Abundant Gene Functions. To understand which microbial genera contribute to metabolic differences between kelp- and turf-dominated reefs, we examined their contributions to differentially abundant metabolic gene functions (Datasets S1–S4). On kelp-dominated reefs, energy metabolism (28%) amino acid metabolism (25%) and cofactor vitamin metabolism (25%) were the most prominent metabolic pathways, followed by genes encoding for carbohydrate metabolism (12%), secondary metabolite metabolism (5%), glycan metabolism (3%), and nucleotide metabolism (2%) (Dataset S3). These genes were present in a diverse range of microbial taxa spanning multiple phyla, indicating that metabolic potential is broadly distributed across the community rather than driven by a single dominant group. On turf-dominated reefs, the differentially abundant metabolic pathways were related to energy (58%) and cofactor (10%) metabolisms, as well as genes related to secondary metabolite (7%), lipid (6%), glycan (5%), nucleotide (5%), carbohydrate vitamin (4%), and amino acid (4%) metabolisms (Dataset S4). Turf-associated functions were primarily driven by *Synechococcus*, which contributed to 18 to 93% of the differentially abundant metabolic genes within each major metabolism.

Microbe–DOM Interactions Differ between Reef States. To explore how microbial communities both influence and respond to their surrounding chemical environment, we utilized LC–MS/MS-based nontargeted metabolomics to characterize DOM pools in summer on kelp- vs. turf-dominated reefs (n = 6 per site; three sites per reef state) that were spatiotemporally paired with our reef biofilm collections. Kelp- and turf-dominated reefs were each uniquely enriched in numerous chemical classes (*SI Appendix*, Fig. S9), highlighting that a shift in the reef metabolome occurs with kelp forest collapse (21). Further, via a Procrustes analysis, we found that microbial community structure and the chemical composition of the DOM pool were spatially correlated (m^2 = 0.88, R = 0.34, P = 0.039) (*SI Appendix*, Table S3), suggesting that–in addition to seaweeds and their waterborne exudates (21)–microbes play a key role in shaping DOM pools in this system. Reciprocally, such a finding also suggests that microbial diversity directly responds to seaweed-induced alterations of the reef metabolome. The metabolome of kelp forests appears to select for metabolically diverse but functionally redundant microbial communities (6), while the metabolome of turf-dominated reefs appears to expand microbial diversity and metabolic potential.

Chemical Composition of DOM Is Related to Ecosystem Function. To assess how the dominant microbes and their biochemical machinery may impact elemental ratios on the reef and thus ecosystem functioning, we first correlated microbial species abundance with individual metabolomic features (unique mass-to-charge-ratios and retention times) (Spearman correlations, P < 0.05 with a Benjamini–Hochberg correction; FDR < 10%) (Figs. 3 and 4 and *SI Appendix*, Fig. S10). Positive correlations imply certain microbes may be linked to the generation or accumulation of specific features, whereas negative correlations imply possible feature removal, feature transformation, or antagonistic relationships. Microbial communities in kelp forests were associated with DOM occupying a distinct region of molecular space, indicating a unique underlying chemical composition relative to turf reefs (*SI Appendix*, Fig. S10). Genera enriched in kelp forests showed strong negative associations with DOM containing high nitrogen content, but positive associations with more reduced carbon (i.e., more negative

Downloaded from https://www.pnas.org by Douglas Rasher on September 2, 2026 from IP address 172.83.249.35.

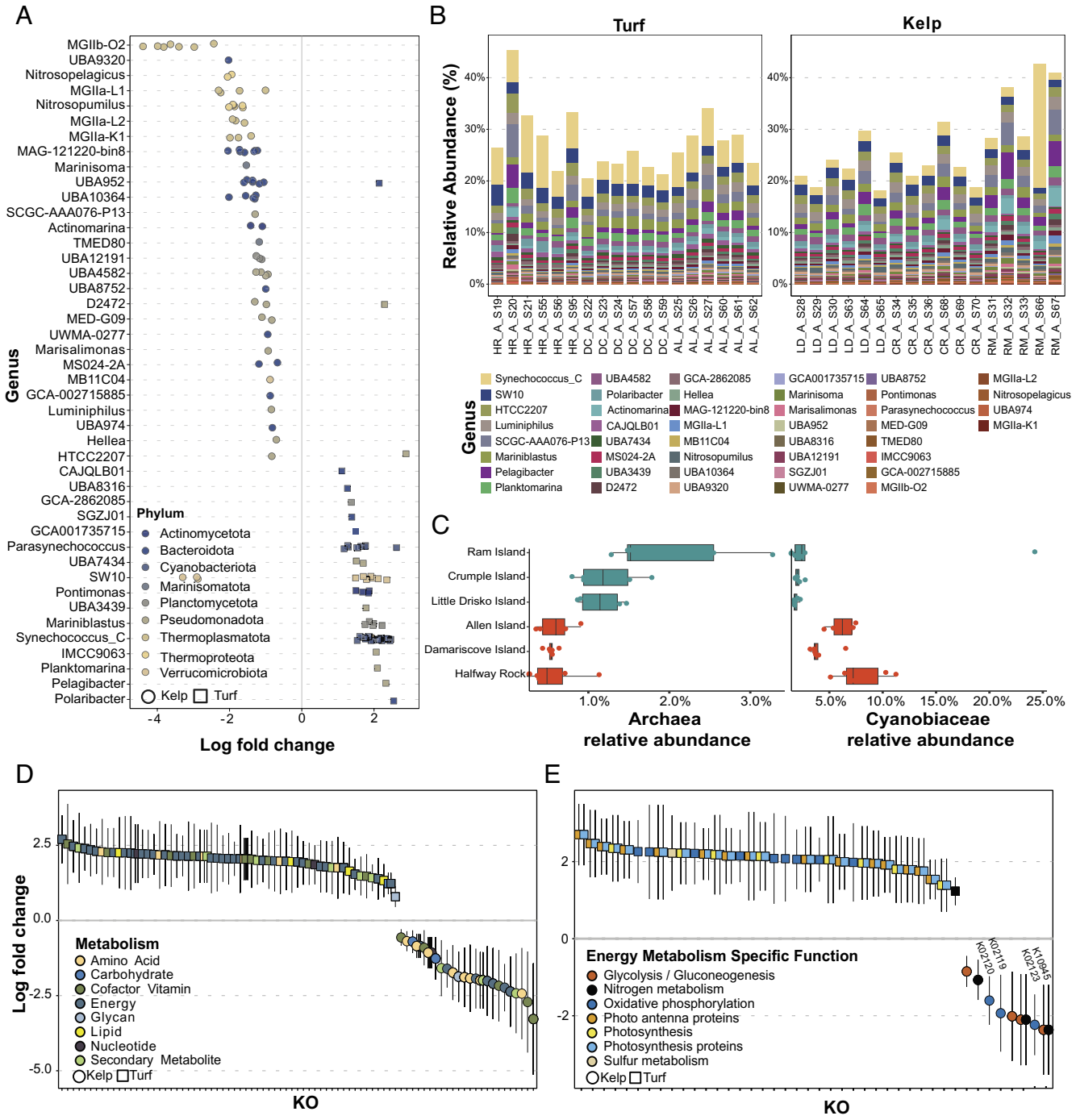


Fig. 2. Differential abundance of microbial genera, metabolic pathways, and energy metabolisms on kelp- vs. turf-dominated reefs. (*A*) Differentially abundant (log2 fold change) microbial genera on kelp-dominated vs. turf-dominated reefs in summer. Color represents the phylum of a given genus. (*B*) Relative abundance of differentially abundant genera between kelp forests and turf reefs. (*C*) Change in relative abundance of Archaea and Cyanobiaceae between kelp forests and turf reefs in summer. (*D*) Differentially abundant (log2 fold change) KEGG Orthology (KO) pathways for microbes on kelp- vs. turf-dominated reefs, related to their metabolisms in summer. Color represents the major metabolism associated with each KO. (*E*) Differentially abundant (log2 fold change) functions within the energy metabolisms of microbes on kelp- and turf-dominated reefs in summer. For panels *A*, *D*, and *E*, circles represent taxa or functions related to kelp-dominated reefs, whereas squares represent taxa or functions related to turf-dominated reefs. Error bars represent the range of all log fold change values observed.

NOSC) (Fig. 3*A*) (27). In contrast, microbes thriving on turf-dominated reefs were positively linked to DOM containing higher oxygen and nitrogen content and more oxidized forms of carbon (i.e., more positive NOSC) (Fig. 3*B*). These patterns suggest that kelp forest microbes are connected to a DOM pool that is rich in nitrogen-containing compounds that are preferentially drawn down or transformed (i.e., creating more reduced compounds), with consistent DOM relationships across the microbial members (Fig. 3*A*). On the other hand, turf reef microbes are connected to a more heterogenous DOM pool, where oxidized, heteroatom-rich compounds covary with microbial abundance, while reduced carbon-rich compounds are often depleted or decoupled (Fig. 3*B*).

Network analysis further revealed that these correlations are not random but organized into structured associations between microbial genera and specific classes of DOM (Fig. 4). By mapping metabolite correlations to predicted chemical classes, we found

Downloaded from https://www.pnas.org by Douglas Rasher on September 2, 2026 from IP address 172.83.249.35.

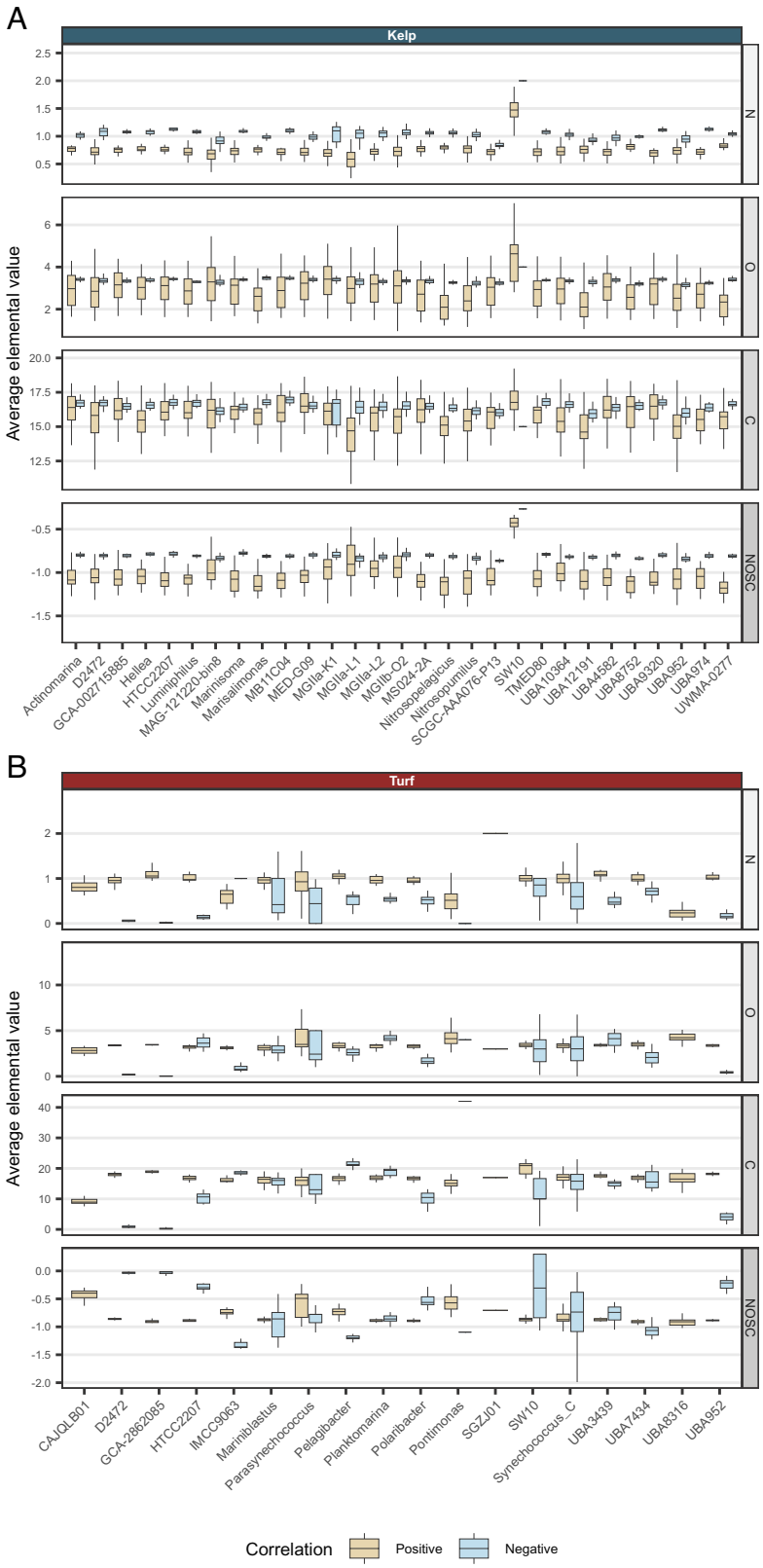


Fig. 3. Associations between abundant microbes and key elements on the reef. Significant Spearman's correlations ($P < 0.05$; FDR < 10%) between microbial genera and individual metabolomic features within kelp forests (*A*) and turf-dominated reefs (*B*). Banner colors indicate the ecosystem state in which each genera (*x* axis) are most abundant (red = turf, blue-green = kelp). Metabolic features were split between those with positive (tan) and negative (light blue) correlations with microbes. All features were grouped by positive and negative correlations, and then the abundance-weighted average number of carbon (C), nitrogen (N), and oxygen (O) atoms, and the nominal oxidation state of carbon (NOSC), were calculated for each sample. Boxplots with lower N, O, C indicate microbial associations with compounds that are low in those elements while higher boxplots indicate compounds with more of that specific element. The sign (positive or negative) of the correlation indicates interaction type (see main text). For NOSC, a more negative value indicates more reduced compounds while a higher value indicates more oxidized compounds. Boxes = interquartile range (IQR); center line = median; whiskers = 1.5× IQR.

Downloaded from https://www.pnas.org by Douglas Rasher on September 2, 2026 from IP address 172.83.249.35.

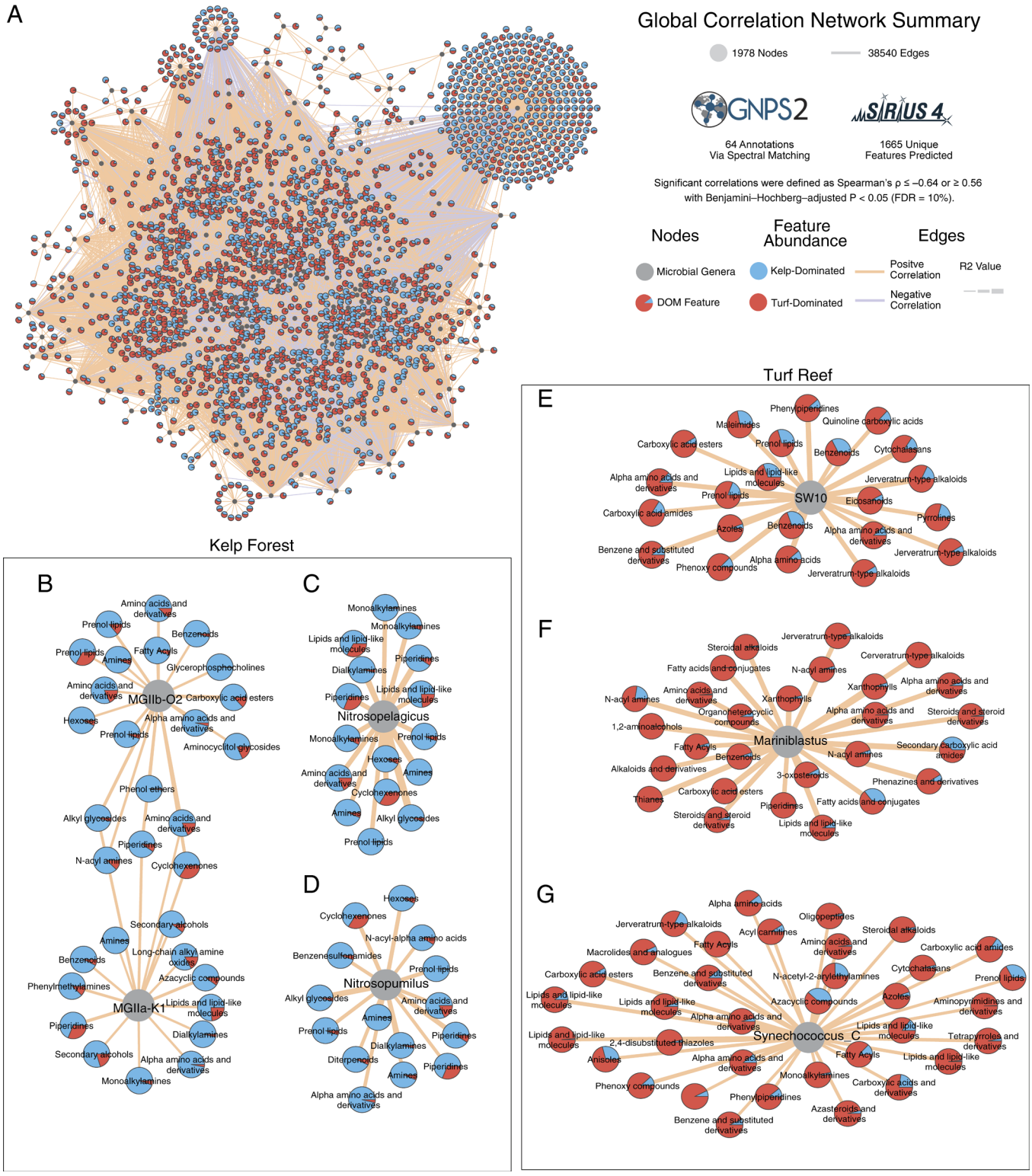


Fig. 4. Microbial genera are linked to distinct classes of DOM across kelp- and turf-dominated reefs. (*A*) Global correlation network between microbial genera (gray nodes) and DOM features (colored nodes). Node pie charts are based on feature abundance in either the turf-dominated (red) or kelp-dominated (blue) ecosystem state. Edges represent significant Spearman correlations (correlation > 0.56 or <–0.64, $P < 0.05$, Benjamini–Hochberg FDR < 10%). Edge color indicates direction of correlation (orange = positive; gray = negative), and width reflects R^2 strength. Subnetwork snapshot views of the top 10 percent of correlations between kelp forest associated microbes *MGIIb-O2* and *MGIIa-K1* (*B*), *Nitrosopelagicus* (*C*), and *Nitrosopumilus* (*D*) and turf associated microbes *SW10* (*E*), *Mariniblastus* (*F*), and *Synechococcus* (*G*). Correlations were subset to the top 10% of R^2 values for both positive and negative correlations. For full view of the species level top 10%, see *SI Appendix*, Fig. S13.

that kelp forest associated microbes were linked to labile and reduced compounds such as lipids and fatty acyls (Fig. 4 *B–D*) (28, 29). In contrast, turf-associated genera were associated with more oxidized metabolite classes, including carboxylic acids, certain amino acids, and benzenoids (Fig. 4 *E–G*) (30–33). These structured patterns support a model in which microbial

Downloaded from https://www.pnas.org by Douglas Rasher on September 2, 2026 from IP address 172.83.249.35.

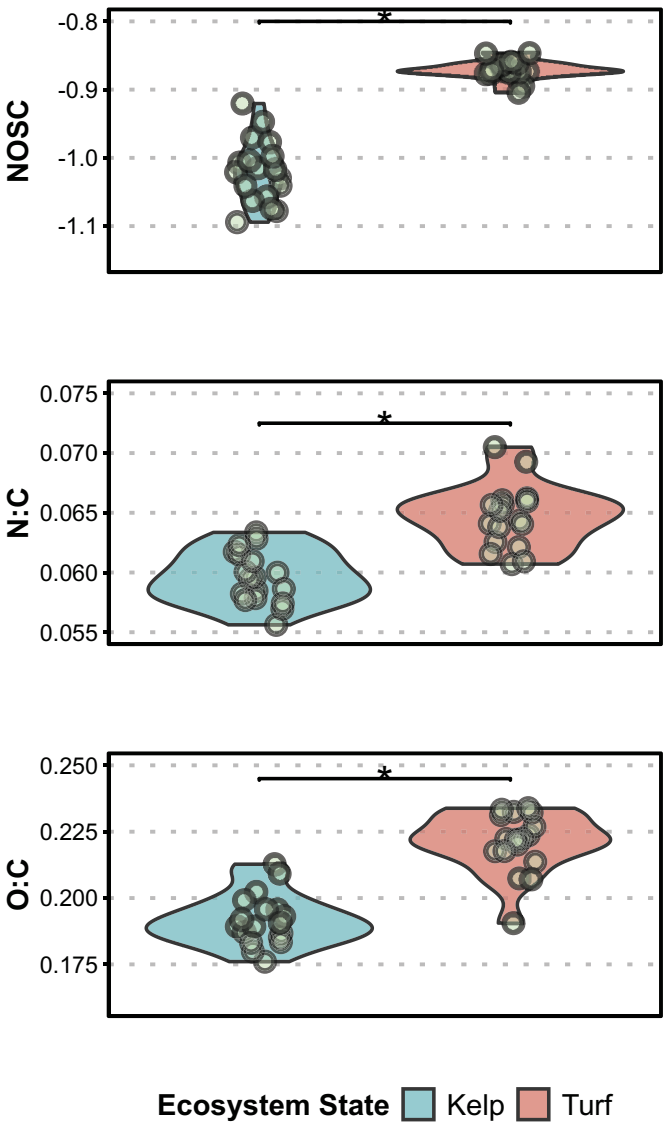


Fig. 5. Kelp forest collapse affects ecosystem functioning through altering DOM pools. Violin plots comparing molecular properties of SPE-extracted DOM collected from 0.5 to 3.0 cm from above the reef. Differentially abundant features were assigned molecular formulas and the nominal oxidation state of carbon (NOSC), oxygen-to-carbon (O:C) ratios, and carbon-to-nitrogen (C:N) ratios were calculated for samples from kelp-dominated (blue-green) vs. turf-dominated (red) reefs (n = 18 samples per state). Green circles are individual samples. Asterisks indicate significant differences (Wilcoxon test, $P < 0.05$).

community composition and metabolic capacity modify the composition and oxidation state of the DOM pool (34, 35).

Next, using the nontargeted metabolomics data, we calculated bulk carbon oxidation ratios of the differentially abundant features found in each ecosystem state, to assess how microbe–DOM linkages may impact ecosystem functionality. Kelp forest DOM contained notably more reduced compounds (–1.019 vs. –0.871) as well as lower O:C ratios (0.191 vs. 0.220) and significantly lower N:C ratios (0.059 vs. 0.064), compared with turf-dominated reefs (Fig. 5). Such findings suggest a shift from a reduced, energy-rich DOM pool in kelp forests to a more oxidized and chemically reworked DOM pool on turf reefs. These elemental ratios are consistent with potential changes in microbial energy yield, carbon processing, and nutrient cycling, although we note that these inferences are based on compositional patterns rather than measurements of process rates (23, 28, 36, 37).

Discussion

Kelp decline and turf proliferation is happening at the warm trailing edge of kelp forest distribution in most temperate ecoregions around the world (7, 9). However, the concomitant impacts on microbial communities and DOM pools are poorly understood. While recent studies have focused on kelp surface-associated microbial communities and ocean warming (38, 39) we took a different approach, examining the microbiome of the reef itself–the "stage" on which key species interactions such as recruitment and competition for space play out in this system. Combining metagenomics and nontargeted metabolomics with robust replication, we show that kelp forest loss leads to significant changes in microbial community structure, metabolic functional potential, and DOM dynamics on the reef. These findings indicate that kelp forest loss has cascading, microbially mediated effects on reef chemistry, underscoring the need to better understand microbial responses to rapid ocean warming.

More specifically, through our spatiotemporally paired data we uncovered specific microbial associations with DOM and document how these interactions shift when kelp is lost. Through pathway reconstruction (40), we found that several of the differentially abundant taxa within kelp forests partition metabolic roles rather than a single dominant metabolic pathway. For example, differences among the *MGII* clades suggest substrate specialization through heterotrophic DOM processing [including glycolysis, a tricarboxylic acid (TCA) cycle, beta-oxidation, and amino acid and cofactor metabolisms], with Thalassarchaeaceae specializing in lipid and fatty acid metabolism and Poseidoniaceae utilizing carbohydrate and glycan processing (Fig. 4*B*) (41, 42). Meanwhile, *Nitrosopumilus* and *Nitrosopelagicus* exhibited metabolic signatures consistent with chemolithoautotrophic ammonia oxidation and inorganic nitrogen cycling, including V/A-type ATP synthase and F420 cofactor biosynthesis but comparatively limited heterotrophic capacity (Fig. 4 *C* and *D*) (43). Together, our results indicate that microbial communities on kelp-dominated reefs are organized around complementary metabolic strategies that couple the turnover of reduced labile organic matter to nitrogen transformations (Figs. 3*A* and 4 *A*–*D*).

This organization shifts markedly on turf-dominated reefs. Turf-associated microbes exhibited metabolic signatures consistent with more oxidative, energy-rich, and biosynthetically active processing of DOM (Fig. 4 *E*–*G*). For example, *SW10* (Akkermansiaceae) encoded the oxidative pentose phosphate pathway and cytochrome c oxidase, indicating strong coupling to aerobic respiration and NADPH production (44). *Mariniblastus* encoded multiple terminal oxidases, ATP synthesis, and pathways for fatty acid elongation, nucleotide biosynthesis, and cofactor production–all consistent with high-energy metabolism and active biomass production (45). Notably, *Synechococcus* further encoded full pathways for carbon fixation, and assimilatory nitrate reduction, indicating that primary production is embedded within this metabolically active network. Together, these features point to a turf microbial community adapted to oxygen-rich conditions and the assimilation of nitrogen and carbon into biomass, consistent with a more oxidized and chemically differentiated DOM pool (Fig. 4 *E*–*G*). This contrasts with kelp-associated microbes and supports the notion that turf-dominated reefs are characterized by greater reworking of DOM, in line with higher N, O, and NOSC values observed in turf-associated metabolites (Figs. 3 and 5).

Similar to microbial dynamics observed in terrestrial ecosystems and on coral reefs, the loss of foundational kelp forests and subsequent shift in microbial taxonomic and functional diversity has implications for ecosystem function (5, 46). Together, the correlation networks

Downloaded from https://www.pnas.org by Douglas Rasher on September 2, 2026 from IP address 172.83.249.35.

(Figs. 3 and 4) and bulk DOM stoichiometry (Fig. 5) suggest that kelp forest microbial assemblages may help retain and recycle nitrogen and labile carbon compounds, reinforcing the ecosystem's high productivity and nutrient retention. Thus, it appears that in addition to their well-established role as structural habitat for macroorganisms, kelp forests provide analogous habitat complexity at microbial scales–creating surfaces, gradients, and key microenvironments (47–49). After the loss of this three-dimensional habitat, diminutive turf algae appear to shift microbial functioning and DOM cycling toward oxidized carbon pools, potentially reducing microbial energy yield and long-term carbon storage (50–52). These shifts in microbe–DOM coupling highlight the ecosystem-level implications of microbial restructuring during state shifts and emphasize the need to better understand how microbial metabolism shapes organic matter fate in coastal ecosystems.

Last, our findings contribute to a growing body of literature demonstrating that foundation species loss due to climate change can have reverberating impacts on ecosystems through altered microbial communities and DOM dynamics (5, 6, 23, 25, 53, 54). As kelp forests decline in areas of rapid warming, such shifts may contribute to changes in ecosystem biodiversity, functioning, and services critical to humans (e.g., fisheries or carbon storage). Understanding how microbial communities respond to—and potentially reinforce—ecosystem state shifts will be essential for predicting ecosystem change, as well as informing strategies to sustain their function in the face of ocean warming and other human-induced disturbances.

Materials and Methods

Site Characterization. To characterize microbial communities and assess how they may vary by ecosystem state, we collected samples at three turf-dominated sites [Halfway Rock (43.65465, −70.03737), Damariscove Island (43.76659, −69.61881), and Allen Island (43.86147, −69.32378)] and three kelp-dominated sites [Ram Island (44.57390, −67.39620), Crumple Island (44.44473, −67.59760), and Little Drisko Island (44.48236, −67.66698)] along the coast of Maine. Samples were collected within a 4-wk period in May–June (hereafter spring), and again within a 4-wk period in August–September (hereafter summer), of 2022. We focused our analyses for this study on the samples collected in summer, as this time period captures the climax state of the reef community in this highly seasonal ecosystem, when algal biomass is at its maximum (14, 16) and when many species of algae, invertebrates, and fishes have recruited or are recruiting to the reef (55, 56). However, we provide characterization of the spring microbial community in the *SI Appendix*.

Microbe Collection. To collect reef biofilms (benthic microbial communities) at each site, divers deployed a 40-m transect along the reef (perpendicular to shore) at 5 to 7 m depth (mean lower low water) and at every 5 m along the transect, used modified "Supersucker" syringes (57) to capture reef-associated microbes. These syringes, which were held flush to the substrate, ejected prefilled sterile seawater to disrupt the benthic biofilm and simultaneously recaptured reef seawater and associated benthic microbes within the 60 mL syringe (n = 6 per site). All samples were stored on ice and brought back to the lab for immediate filtration. Between sampling events, Supersuckers were triple rinsed with hydrochloric acid (10%) and MilliQ water to prevent contamination. One sample was lost during our summer collection efforts (from a kelp-dominated site).

DNA Filtration, Extraction, and Sequencing. Individual samples were filtered on 0.2 μm cellulose nitrate filters and stored in 5 mL tubes at –80 °C until extraction. We used a DNEasy PowerSoil Pro kit (Qiagen, Germany) to extract the DNA from each filter, following the manufacturer's guidelines. DNA was eluted using 60 μL of elution buffer. All samples were diluted to a concentration of 1 ng μL^{-1} and sent to the Hubbard Center for Genome Studies at the University of New Hampshire for shotgun metagenomic sequencing. DNA libraries were made using a Kapa HyperPlus DNA kit (Roche Molecular Systems, USA) and samples were split into three runs on a NovaSeq 6000 SP PE sequencer (Illumina, USA). Samples from all sites and seasons were interspersed across all three runs so as to not confound the effects of ecosystem state or season with batch-to-batch variance (~4 million paired-end reads per sample per run, ~12 million total).

Metagenomic Bioinformatics. For detailed bioinformatics refer to the *SI Appendix*. Briefly, reads from the three runs were concatenated into one read file per sample. Metagenome assembled genomes (MAGs) were produced (607 in total) and added to 4,675 single amplified genomes (SAGS) previously collected from the Gulf of Maine (58–60; Dataset S5) and were annotated using GTDB-tk (v2.5.2 against the r226 database (61). Assemblies were clustered into species-like units (>95% ANI) (62).

All assemblies were translated into protein sequences and concatenated into one amino acid fasta file for dereplication (63, 64). Sequences were annotated against the KEGG Orthology HMM profiles with a single classification chosen per sequence by lowest e-value (65, 66). Amino acid sequences were converted into a Kaiju database with the quality control reads that were used to create the MAGs mapped to the Kaiju database with a modification of the GORG-classifier pipeline (60, 67, 68). The species-like (>95% ANI) unit classification (both taxonomic and functional annotations) were added as metadata to each nonredundant protein sequence. We only retained reads that unambiguously mapped to a single species unit–reads that only had one match, or multiple matches that were within the same "species" cluster–which was roughly 80% of classified reads (*SI Appendix*, Figs. S11 and S12).

Metagenomic Statistical Analysis. Relative abundance: To visualize differences in microbial community composition across samples, we generated relative abundance bar plots. Low-prevalence features are often driven by sequencing artifacts, contamination, or stochastic detection and can inflate variance and reduce statistical power. Consistent with common practice, we thus removed features present in <10% of samples, which reduces noise while retaining biologically meaningful taxa (69, 70). The filtered count data were then normalized by calculating row-wise proportions, representing the relative abundance of each feature within a given sample and summarized by kelp- vs. turf-dominated ecosystem states.

Core communities (taxa and functions): To identify core microbial families associated with kelp and turf-dominated states, we calculated the relative abundance of microbial families within each sample and defined core families as those consistently present at > 5% relative abundance in at least 70% of the samples within each reef state. We also examined core functional features associated with kelp- and turf-dominated reefs. Functional annotations (KOs) were grouped by their respective samples and normalized using relative abundances. Core functions were defined as those consistently present at > 1% relative abundance in at least 70% of the samples within each reef state.

Ordinations: To assess differences in microbe taxonomy and function on kelp- vs. turf-dominated reefs, statistical tests were performed on count tables derived from species-level taxonomy and functional annotations from the KEGG database. Low-abundance features, defined as those present in < 10% of the samples, were removed prior. The remaining count tables were transformed to address the compositional nature of sequence count data (71). Using a center log-ratio (CLR) normalization, zeros were first imputed using a count-zero multiplicative replacement (CZM) approach. After log transformation, the data were centered by subtracting the mean of the log-transformed values.

The CLR-transformed count data were used to calculate sample-to-sample Aitchison distance matrices based on Euclidean distances. Ordination was performed using Principal Coordinates Analysis (PCoA) to visualize clustering patterns. To test for significant differences between groups, permutational multivariate ANOVA (PERMANOVA) was conducted using the *adonis2* function, and homogeneity of group dispersions was assessed using the *betadisper* function (*SI Appendix*, Tables S1 and S2) (72).

Differential abundance: Differentially abundant components, including taxonomic and functional annotations, that contributed to observed clustering patterns were identified using compositionally aware differential abundance tools, as recommended for compositional data (71, 73). Two tools were used for this analysis: Aldex2 and ANCOMBC2 (74). Components identified by both methods were filtered based on an adjusted *P*-value threshold of $P < 0.05$. We focused downstream interpretations on features that were consistently identified as significant by both Aldex2 and ANCOMBC2, following established recommendations for differential

Downloaded from https://www.pnas.org by Douglas Rasher on September 2, 2026 from IP address 172.83.249.35.

abundance analyses (73). Last, to test if the compositional analysis framework was robust and consistent with other methods, and account for variation in both gene length and sequencing depth, KEGG Orthology (KO) level relative abundance was calculated using a modified reads per kilobase per million approach (RPKM). The outputs of this exercise can be found in the *SI Appendix*, Fig. S14).

Water Sampling for Nontargeted Metabolomics. To characterize the dissolved organic matter (DOM) pool of each site in the summer, we collected water samples and subjected them to nontargeted metabolomics. Water (1 L, n = 6 per site) and microbial (see above) samples were collected from the same six locations at each site, making them spatially linked. Water samples were collected from 0.5 to 3.0 centimeters above the benthos, using a custom-designed organic matter sampler (21). Samples were brought to the surface, stored on ice, and transported to the lab to be immediately filtered and extracted. To avoid contamination, bottles were cleaned with 10% HCl (trace metal grade), methanol (LC–MS grade), and MilliQ water between each sampling event. All glassware used during extractions were triple rinsed with methanol (LC–MS grade) and MilliQ water and then precombusted for 4 h at 450 °C.

Seawater Metabolite Extraction. DOM samples were individually extracted using previously established and described methods (21) (for detailed information, see *SI Appendix*). Briefly, each 1 L water sample was passed through an activated solid phase extraction (SPE) Priority PolLutant (PPL) cartridge (Agilent, Germany) and dried under N_2 gas. SPE Cartridges were frozen at −80 °C until elution, at which point cartridges were eluted with 2 mL of methanol in a precleaned and pre-weighed HPLC vial. Procedural blanks (to assess contamination) were created by repeating the sample preparation and extraction process with water (LC–MS grade) only.

Nontargeted UHPLC-MS/MS Analysis. DOM samples were redissolved in 100 μL methanol and 1% formic acid, then subjected to ultra-high-performance liquid-chromatography tandem mass spectrometry (UHPLC-MS/MS). Two standards were also created and analyzed to account for instrument drift and batch effects. Samples were randomized before analysis. We subjected our samples to UHPLC-MS/MS using a Q Exactive HF Orbitrap mass spectrometer coupled to a Vanquish Horizon UHPLC and reverse phase C18 column, with settings previously described (75) (see details in the *SI Appendix*).

Metabolomics Bioinformatics. Before postprocessing, the six compounds that comprised the internal positive control were assessed for shifts in mass to charge (m/z) and retention time (RT); those values were then accounted for in feature picking using mzmine (see below) (21). Thermo.raw datasets were converted to *.mzML* in centroid mode using MSConvert (76).

Centroided data were processed in batch mode with mzmine (4.5.0) for feature extraction, characterization, and quantification (77). SIRIUS (6.1.0) was used to annotate molecular formulas and compound classes from tandem mass spectra (78–80). To annotate DOM features, we used the GNPS2 Featured-based molecular networking workflow (81). Parameters were as follows: Fragment tolerance 0.01, Network min cosine 0.7, and network min matched peaks 6.

Metabolomics Statistical Analysis. The feature table–the output of mzmine–was further refined using a postprocessing script from the FBMN-STATS workflow (82). To eliminate background noise, we conducted feature removal using our blank samples. Features were removed if the average contribution in the blank samples compared to the environmental samples surpassed a 10% threshold. We imputed values to a low baseline threshold. To establish the baseline cutoff, we identified the minimum nonzero value in the feature table, which represented the lowest detectable signal above background noise. This threshold ensured that only meaningful abundance values were considered in downstream analyses, avoiding potential artifacts introduced by zero values.

Correlation Analysis of Microbial Abundances and DOM Features. Relative abundances of differentially abundant microbial species were correlated with metabolomic features using the Corromics Correlation App (82). Spearman's correlation coefficients were computed to evaluate the strength and direction of monotonic relationships between microbial relative abundances and the signal intensities of individual DOM features. Significance of correlations were determined using a *P*-value threshold of < 0.05. To account for multiple comparisons, *P*-values were adjusted using the Benjamini–Hochberg procedure, and only correlations with a false discovery rate (FDR) $< 10\%$ were considered significant (82). For groups of features showing significant positive or negative correlations with microbes, elemental compositions (C, N, O) and nominal oxidation state of carbon (NOSC) were calculated based on the assigned molecular formulas from SIRIUS.

Finally, pathway reconstructions were generated from the MAG and SAG data for the most differentially abundant species using the KEGG reconstruct tool (40, 60). These reconstructions were integrated with the correlation results to elucidate the metabolic pathways that may underlie the observed relationships between microbial community composition and DOM characteristics.

Elemental Ratios and Ecosystem Function. Differentially abundant DOM features were determined through a log fold change test with a Benjamini–Hochberg correction ($P < 0.05$). The average weighted feature abundance was calculated for the elemental ratios and NOSC calculated above for features from turf- and kelp-dominated reefs.

Data, Materials, and Software Availability. Metagenomic data, metadata, metabolomic data, code data have been deposited in Dryad/NCBI [Dryad (https://doi.org/10.5061/dryad.79cnp5j78) (40) NCBI (PRJNA1264483) (83)]. Previously published data were used for this work (84).

ACKNOWLEDGMENTS. We thank Stuart Ryan, Phoebe Churney, and Rene Francolini for help in the field, and Tilman Schramm, Karoline Steuer-Lodd, and Stilianos Papadopoulos Lambidis for help with LC–MS/MS data acquisition and analysis. We thank Bigelow Laboratory for Ocean Sciences for logistical support. This work was conducted with permission from the Maine Department of Marine Resources (special license 2022-36-03). This project was supported through an NSF cooperative agreement award (OIA-1489227) given to the University of Maine from the EPSCoR RII Track-1 program (P.D.C., D.C.B., and D.B.R.), a Louise H. & David S. Ingalls Foundation grant (D.B.R.), the German Research Foundation through the CMFI cluster of Excellence (EXC 2124-390838134, D.P.), an Essex Avenue Foundation grant (D.C.B.), and a PADI Foundation Fellowship (S.P.F.). Raw metagenomic data and metagenome assemblies can be found at NCBI (83). Raw metabolomics data can be found on Dryad (84). All other data, code, and command files for this study are on Dryad (40).

Author affiliations: [a]Bigelow Laboratory for Ocean Sciences, East Boothbay, ME 04544; [b]Darling Marine Center, University of Maine, Walpole, ME 04573; [c]Department of Biochemistry, University of California, Riverside, CA 92521; and [d]Interfaculty Institute of Microbiology and Infection Medicine, University of Tübingen, Tübingen 72076, Germany

1. A.-S. Crépin, R. Biggs, S. Polasky, M. Troell, A. De Zeeuw, Regime shifts and management. *Ecol. Econ.* **84**, 15–22 (2012).
2. M. Scheffer, S. R. Carpenter, Catastrophic regime shifts in ecosystems: Linking theory to observation. *Trends Ecol. Evol.* **18**, 648–656 (2003).
3. M. Scheffer, S. Carpenter, J. A. Foley, C. Folke, B. Walker, Catastrophic shifts in ecosystems. *Nature* **413**, 591–596 (2001).
4. S. D. Ling *et al.*, Global regime shift dynamics of catastrophic sea urchin overgrazing. *Philos. Trans. R. Soc. B Biol. Sci.* **370**, 20130269 (2015).
5. A. F. Haas *et al.*, Global microbialization of coral reefs. *Nat. Microbiol.* **1**, 16042 (2016).
6. C. E. Nelson, L. Wegley Kelly, A. F. Haas, Microbial interactions with dissolved organic matter are central to coral reef ecosystem function and resilience. *Annu. Rev. Mar. Sci.* **15**, 431–460 (2023).
7. K. Filbee-Dexter, T. Wernberg, Rise of turfs: A new battlefront for globally declining kelp forests. *BioScience* **68**, 64–76 (2018).
8. T. Wernberg *et al.*, An extreme climatic event alters marine ecosystem structure in a global biodiversity hotspot. *Nat. Clim. Change* **3**, 78–82 (2013).
9. A. Pessarrodona *et al.*, Homogenization and miniaturization of habitat structure in temperate marine forests. *Glob. Change Biol.* **27**, 5262–5275 (2021).
10. L. Benedetti-Cecchi *et al.*, Predicting the consequences of anthropogenic disturbance: Large-scale effects of loss of canopy algae on rocky shores. *Mar. Ecol. Prog. Ser.* **214**, 137–150 (2001).
11. B. K. Eriksson, G. Johansson, P. Snoeijs, Long-term changes in the macroalgal vegetation of the inner Gullmar Fjord, Swedish Skagerrak coast. *J. Phycol.* **38**, 284–296 (2002).
12. F. E. Moy, H. Christie, Large-scale shift from sugar kelp (*Saccharina latissima*) to ephemeral algae along the south and west coast of Norway. *Mar. Biol. Res.* **8**, 309–321 (2012).
13. C. J. Feehan, S. P. Grace, C. A. Narvaez, Ecological feedbacks stabilize a turf-dominated ecosystem at the southern extent of kelp forests in the Northwest Atlantic. *Sci. Rep.* **9**, 7078 (2019).
14. T. S. Suskiewicz *et al.*, Ocean warming undermines the recovery resilience of New England kelp forests following a fishery-induced trophic cascade. *Ecology* **105**, e4334 (2024).
15. J. A. Dijkstra *et al.*, Invasive seaweeds transform habitat structure and increase biodiversity of associated species. *J. Ecol.* **105**, 1668–1678 (2017).

Downloaded from https://www.pnas.org by Douglas Rasher on September 2, 2026 from IP address 172.83.249.35.

16. S. P. Farrell *et al.*, From kelp forests to turf reefs: Patterns, drivers, and impacts to functional diversity. *Ecology* **107**, e70408 (2026).
17. A. Pessarrodona *et al.*, Global seaweed productivity. *Sci. Adv.* **8**, eabn2465 (2022).
18. A. Pessarrodona *et al.*, Tropicalization unlocks novel trophic pathways and enhances secondary productivity in temperate reefs. *Funct. Ecol.* **36**, 659–673 (2022).
19. J. A. Dijkstra, A. Litterer, K. Mello, B. S. O'Brien, Y. Rzhanov, Temperature, phenology, and turf macroalgae drive seascape change: Connections to mid-trophic level species. *Ecosphere* **10**, e02923 (2019).
20. B. S. O'Brien, K. Mello, A. Litterer, J. A. Dijkstra, Seaweed structure shapes trophic interactions: A case study using a mid-trophic level fish species. *J. Exp. Mar. Biol. Ecol.* **506**, 1–8 (2018).
21. S. P. Farrell *et al.*, Turf algae redefine the chemical landscape of temperate reefs, limiting kelp forest recovery. *Science* **388**, 876–880 (2025).
22. C. A. Carlson, D. A. Hansell, "DOM sources, sinks, reactivity, and budgets" in *Biogeochemistry of Marine Dissolved Organic Matter*, D. A. Hansell, C. A. Carlson, Eds. (Academic Press, 2015), pp. 65–126.
23. L. Wegley Kelly *et al.*, Distinguishing the molecular diversity, nutrient content, and energetic potential of exometabolomes produced by macroalgae and reef-building corals. *Proc. Natl. Acad. Sci. U.S.A.* **119**, e2110283119 (2022).
24. T. N. F. Roach *et al.*, A multiomic analysis of *in situ* coral–turf algal interactions. *Proc. Natl. Acad. Sci. U.S.A.* **117**, 13588–13595 (2020).
25. D. A. Wardle *et al.*, Ecological linkages between aboveground and belowground biota. *Science* **304**, 1629–1633 (2004).
26. S. J. Giovannoni, C. Thrash, B. Temperton, Implications of streamlining theory for microbial ecology. *ISME J.* **8**, 1553–1565 (2014).
27. D. E. LaRowe, P. V. Cappellen, Degradation of natural organic matter: A thermodynamic analysis. *Geochim. Cosmochim. Acta* **75**, 2030–2042 (2011).
28. Z. Quinlan *et al.*, Microbial community metabolism of coral reef exometabolomes broadens the chemodiversity of labile dissolved organic matter. *Environ. Microbiol.* **27**, e70064 (2025).
29. E. Canuel, C. Martens, Reactivity of recently deposited organic matter: Degradation of lipid compounds near the sediment–water interface. *Geochim. Cosmochim. Acta* **60**, 1793–1806 (1996).
30. S. Liu *et al.*, Different carboxyl-rich alicyclic molecules proxy compounds select distinct bacterioplankton for oxidation of dissolved organic matter in the mesopelagic Sargasso Sea. *Limnol. Oceanogr.* **65**, 1532–1553 (2020).
31. A. Gunina, A. Smith, Y. Kuzyakov, D. Jones, Microbial uptake and utilization of low molecular weight organic substrates in soil depend on carbon oxidation state. *Biogeochemistry* **133**, 89–100 (2017).
32. A. Gunina, Y. Kuzyakov, From energy to (soil organic) matter. *Glob. Change Biol.* **28**, 2169–2182 (2022).
33. J. Clamp, L. Hough, The periodate oxidation of amino acids with reference to studies on glycoproteins. *Biochem. J.* **94**, 17–24 (1965).
34. K. Kajan, H. Osterholz, J. Stegen, G. Udovič, S. Orlić, Mechanisms shaping dissolved organic matter and microbial community in lake ecosystems. *Water Res.* **245**, 120653 (2023).
35. Y. Li *et al.*, Oxygen availability regulates the quality of soil dissolved organic matter by mediating microbial metabolism and iron oxidation. *Glob. Change Biol.* **28**, 7410–7427 (2022).
36. B. Mueller *et al.*, Nocturnal dissolved organic matter release by turf algae and its role in the microbialization of reefs. *Funct. Ecol.* **36**, 2104–2118 (2022).
37. E. Freeman *et al.*, Universal microbial reworking of dissolved organic matter along environmental gradients. *Nat. Commun.* **15**, 187 (2022).
38. B. L. Weigel, C. A. Pfister, Successional dynamics and seascape-level patterns of microbial communities on the canopy-forming kelps *Nereocystis luetkeana* and *Macrocystis pyrifera*. *Front. Microbiol.* **10**, 346 (2019).
39. B. L. Weigel, K. K. Miranda, E. C. Fogarty, A. R. Watson, C. A. Pfister, Functional insights into the kelp microbiome from metagenome-assembled genomes. *mSystems* **7**, e01422-21 (2022).
40. S. P. Farrell *et al.*, Kelp forest collapse alters the reef microbiome and associated metabolome. Dryad. https://doi.org/10.5061/dryad.79cnp5j78. Deposited 4 August 2026.
41. J. Damashek, Transcriptional activity differentiates families of Marine Group II Euryarchaeota in the coastal ocean. *ISME Commun.* **1**, 5 (2021).
42. C. Rinke *et al.*, A phylogenomic and ecological analysis of the globally abundant marine group II archaea (Ca. *Poseidoniales* ord. nov.). *ISME J.* **13**, 663–675 (2018).
43. C. Walker *et al.*, *Nitrosopumilus maritimus* genome reveals unique mechanisms for nitrification and autotrophy in globally distributed marine crenarchaea. *Proc. Natl. Acad. Sci. U.S.A.* **107**, 8818–8823 (2010).
44. T. TeSlaa, M. Ralser, J. Fan, J. Rabinowitz, The pentose phosphate pathway in health and disease. *Nat. Metab.* **5**, 1275–1289 (2023).
45. L. Nikkanen, D. Solymosi, M. Jokel, Y. Allahverdiyeva, Regulatory electron transport pathways of photosynthesis in cyanobacteria and microalgae: Recent advances and biotechnological prospects. *Physiol. Plant.* **173**, 514–525 (2021).
46. M. W. I. Schmidt, Persistence of soil organic matter as an ecosystem property. *Nature* **478**, 49–56 (2011).
47. S. Ramírez-Puebla *et al.*, Spatial organization of the kelp microbiome at micron scales. *Microbiome* **10**, 52 (2022).
48. C. Pfister, M. Altabet, B. Weigel, Kelp beds and their local effects on seawater chemistry, productivity, and microbial communities. *Ecology* **100**, e02798 (2019).
49. H. Teagle, S. Hawkins, P. Moore, D. Smale, The role of kelp species as biogenic habitat formers in coastal marine ecosystems. *J. Exp. Mar. Biol. Ecol.* **492**, 81–98 (2017).
50. D. L. Kirchman, "Degradation of organic matter" in *Processes in Microbial Ecology* (Oxford University Press, 2018), pp. 113–132.
51. X. Qu *et al.*, Deforestation impacts soil biodiversity and ecosystem services worldwide. *Proc. Natl. Acad. Sci. U.S.A.* **121**, e2318475121 (2024).
52. M. I. Behnke *et al.*, Aquatic biomass is a major source to particulate organic matter export in large Arctic rivers. *Proc. Natl. Acad. Sci. U.S.A.* **120**, e2209883120 (2023).
53. L. Wegley Kelly *et al.*, Molecular commerce on coral reefs: Using metabolomics to reveal biochemical exchanges underlying holobiont biology and the ecology of coastal ecosystems. *Front. Mar. Sci.* **8**, 630799 (2021).
54. J. R. Zaneveld *et al.*, Overfishing and nutrient pollution interact with temperature to disrupt coral reefs down to microbial scales. *Nat. Commun.* **7**, 11833 (2016).
55. R. Wahle, R. Steneck, Recruitment habitats and nursery grounds of the American lobster *Homarus americanus*: A demographic bottleneck? *Mar. Ecol. Prog. Ser.* **69**, 231–243 (1991).
56. F. P. Ojeda, J. H. Dearborn, Diversity, abundance, and spatial distribution of fishes and crustaceans in the rocky subtidal zone of the Gulf of Maine. *Fish. Bull.* **88**, 403–410 (1985).
57. Y. W. Lim *et al.*, Sequencing at sea: Challenges and experiences in ion torrent PGM sequencing during the 2013 Southern Line Islands research expedition. *PeerJ* **2**, e520 (2014).
58. P. A. Ewels *et al.*, The nf-core framework for community-curated bioinformatics pipelines. *Nat. Biotechnol.* **38**, 276–278 (2020).
59. S. Krakau, D. Straub, H. Gourlé, G. Gabernet, S. Nahnsen, nf-core/mag: A best-practice pipeline for metagenome hybrid assembly and binning. *NAR Genom. Bioinform.* **4**, lqac007 (2022).
60. J. H. Munson-McGee *et al.*, Decoupling of respiration rates and abundance in marine prokaryoplankton. *Nature* **612**, 764–770 (2022).
61. P.-A. Chaumeil, A. J. Mussig, P. Hugenholtz, D. H. Parks, GTDB-Tk v2: Memory friendly classification with the genome taxonomy database. *Bioinformatics* **38**, 5315–5316 (2022).
62. M. R. Olm, C. T. Brown, B. Brooks, J. F. Banfield, dRep: A tool for fast and accurate genomic comparisons that enables improved genome recovery from metagenomes through de-replication. *ISME J.* **11**, 2864–2868 (2017).
63. T. Seemann, Prokka: Rapid prokaryotic genome annotation. *Bioinformatics* **30**, 2068–2069 (2014).
64. M. Steinegger, J. Söding, MMseqs2 enables sensitive protein sequence searching for the analysis of massive data sets. *Nat. Biotechnol.* **35**, 1026–1028 (2017).
65. R. D. Finn, J. Clements, S. R. Eddy, HMMER web server: Interactive sequence similarity searching. *Nucleic Acids Res.* **39**, W29–W37 (2011).
66. M. Kanehisa, M. Furumichi, Y. Sato, M. Kawashima, M. Ishiguro-Watanabe, KEGG for taxonomy-based analysis of pathways and genomes. *Nucleic Acids Res.* **51**, D587–D592 (2023).
67. P. Menzel, K. L. Ng, A. Krogh, Fast and sensitive taxonomic classification for metagenomics with Kaiju. *Nat. Commun.* **7**, 11257 (2016).
68. J. Brown, J. Brown, gorg-classifier (Version 1.1.0). Zenodo (2026). https://doi.org/10.5281/zenodo.19456322. Accessed 4 June 2026.
69. Q. Cao *et al.*, Effects of rare microbiome taxa filtering on statistical analysis. *Front. Microbiol.* **11**, 607325 (2021).
70. M. Nikodémová *et al.*, The effect of low-abundance OTU filtering methods on the reliability and variability of microbial composition assessed by 16S rRNA amplicon sequencing. *Front. Cell. Infect. Microbiol.* **13**, 1165295 (2023).
71. G. B. Gloor, J. M. Macklaim, V. Pawlowsky-Glahn, J. J. Egozcue, Microbiome datasets are compositional: And this is not optional. *Front. Microbiol.* **8**, 2224 (2017).
72. P. J. McMurdie, S. Holmes, phyloseq: An R package for reproducible interactive analysis and graphics of microbiome census data. *PLoS One* **8**, e61217 (2013).
73. J. T. Nearing *et al.*, Microbiome differential abundance methods produce different results across 38 datasets. *Nat. Commun.* **13**, 342 (2022).
74. A. D. Fernandes *et al.*, Unifying the analysis of high-throughput sequencing datasets: Characterizing RNA-seq, 16S rRNA gene sequencing and selective growth experiments by compositional data analysis. *Microbiome* **2**, 15 (2014).
75. D. Petras *et al.*, High-resolution liquid chromatography tandem mass spectrometry enables large scale molecular characterization of dissolved organic matter. *Front. Mar. Sci.* **4**, 405 (2017).
76. R. Adusumilli, P. Mallick, "Data conversion with ProteoWizard msConvert" in *Proteomics*, L. Comai, J. E. Katz, P. Mallick, Eds. (Springer, 2017), pp. 339–368.
77. R. Schmid *et al.*, Integrative analysis of multimodal mass spectrometry data in MZmine 3. *Nat. Biotechnol.* **41**, 447–449 (2023).
78. K. Dührkop *et al.*, SIRIUS 4: A rapid tool for turning tandem mass spectra into metabolite structure information. *Nat. Methods* **16**, 299–302 (2019).
79. K. Dührkop, H. Shen, M. Meusel, J. Rousu, S. Böcker, Searching molecular structure databases with tandem mass spectra using CSI:FingerID. *Proc. Natl. Acad. Sci. U.S.A.* **112**, 12580–12585 (2015).
80. H. W. Kim *et al.*, NPClassifier: A deep neural network-based structural classification tool for natural products. *J. Nat. Prod.* **84**, 2795–2807 (2021).
81. L.-F. Nothias *et al.*, Feature-based molecular networking in the GNPS analysis environment. *Nat. Methods* **17**, 905–908 (2020).
82. A. K. Pakkir Shah *et al.*, Statistical analysis of feature-based molecular networking results from non-targeted metabolomics data. *Nat. Protoc.* **20**, 92–162 (2024).
83. S. P. Farrell *et al.*, Kelp forest collapse alters the reef microbiome and associated metabolome. NCBI BioProject. https://www.ncbi.nlm.nih.gov/bioproject?LinkName=biosample_bioproject&from_uid=48554398&log$=activity. Deposited 17 May 2026.
84. S. P. Farrell *et al.*, Turf algae redefine the chemical landscape of temperate reefs, limiting kelp forest recovery. Dryad. https://doi.org/10.5061/dryad.kd51c5bhd. Accessed 4 August 2026.

Downloaded from https://www.pnas.org by Douglas Rasher on September 2, 2026 from IP address 172.83.249.35.